Quasi-biennial oscillation disrupted by abnormal Southern Hemisphere stratosphere

James A. Anstey[1]*, Timothy P. Banyard[2], Neal Butchart[3], Lawrence Coy[4,5], Paul A. Newman[4], Scott Osprey[6,7], Corwin J. Wright[2]

[1]Canadian Centre for Climate Modelling and Analysis, Environment and Climate Change Canada, Victoria, Canada

[2]Centre for Space, Atmospheric and Oceanic Science, University of Bath, Bath, UK

[3]Met Office Hadley Centre, Reading, United Kingdom

[4]NASA Goddard Space Flight Center Greenbelt, Maryland, USA

[5]SSAI, Lanham, Maryland, USA

[6]National Centre for Atmospheric Science, Oxford, United Kingdom

[7]Department of Physics, University of Oxford, Oxford, United Kingdom

Corresponding author: James Anstey, `james.anstey@canada.ca`

Abstract

The quasi-biennial oscillation (QBO) is a repeating cycle of tropical stratosphere winds reversing direction from eastward to westward roughly every 14 months[1]. Discovered independently by British[2] and American[3] scientists the QBO continued uninterrupted for 27 cycles from 1953 until February 2016 when a westward jet unexpectedly formed in the lower stratosphere during the eastward phase[4,5]. This disruption is attributed to unusually high wave-momentum fluxes from the Northern Hemisphere[5,6]. A second, similar, QBO disruption occurred during the 2019/2020 northern winter though wave fluxes from the Northern Hemisphere were weak. Here we show that this latest disruption to the regular QBO cycling was stronger than that seen in 2016 and resulted from horizontal momentum transport from the Southern Hemisphere during abnormal winter conditions[7,8]. In both disruptions the normal downward progression of the QBO halts and the eastward shear zone above the disruption moves upward assisted by stronger tropical upwelling during the boreal winter. The predictable signal associated with the QBO's quasi-regular phase progression is permanently lost during disruptions and the oscillation reemerges after a few months significantly shifted in phase from what would be expected if the phase had progressed uninterrupted. We infer from an increased wave-momentum flux into equatorial latitudes seen in model climate projections supporting the latest Intergovernmental Panel on Climate Change (IPCC) assessment that disruptions to the QBO are likely to be more common in future. Consequently, we anticipate that in future the QBO will be a less reliable source of predictability on lead times extending out to several years than it currently is.

Main

The QBO consists of alternating layers of eastward and westward wind that emerge above 40 km and gradually descend through the tropical stratosphere before dissipating near the tropopause (16 km)[9]. Observed periods of this irregular oscillation range from 22 to 35 months averaging around 28 months[10]. The QBO dominates stratospheric variability in the tropics while modulating variability in mid to high latitudes[11] and thereby provides a useful source of predictability on seasonal-to-decadal timescales[12]. The established QBO fluid dynamical mechanism, or canonical model, involves vertically propagating waves from the troposphere that accelerate the winds through interactions with the winds themselves[1]. This leads to the descending layers of winds of opposite sign (Fig. 1a).

Opposing the downward progression is tropical upwelling[13] from the Brewer-Dobson circulation[14]. It was thought, at least until recently, that horizontally propagating waves from the mid-latitudes into the tropics played only a minor part in the QBO's evolution[15] - explaining the QBO's remarkable cycle-to-cycle consistency, with predictability extending out to a few years[12]. Moreover, the oscillation's deep vertical structure allows 90% of the month-to-month variability of the QBO to be described by just two vertical structure modes (Empirical Orthogonal Functions, or EOFs[16]; Methods), and the highly predictable QBO signal is associated with the time evolution of the amplitude of these two modes.

Conventional wisdom was challenged in February 2016 when the usual QBO cycling was disrupted[4–6,17] for the first time since its discovery in the early 1960s[2,3]. A vertically thin layer of westward winds appeared at 40 hPa, within a decaying eastward QBO phase (Fig. 1a). Anomalous westward acceleration resulted from unusually large horizontal fluxes of wave-momentum from the Northern Hemisphere (NH)[5], linked to the occurrence of a very large El Niño event[17,18]. Conditions in the subtropics contributed to focusing the wave activity into the QBO jet[19,20]. Failures by models to predict the disruption[5] are consistent with it originating in the extratropics since predictability timescales are shorter there than in the tropics. The abnormal westward winds at 40 hPa subsequently strengthened, descended, and the QBO returned to its usual cycling by early 2017 (Fig. 1a).

A second QBO disruption began in December 2019, only four years after the previous event and without a strong El Niño being present. Here we compare the recent event to the previous one and examine their causes. We use future projections from climate models to assess whether QBO disruptions are an emerging signal of climate change, and consider the implications of these events when using the QBO as a source of predictability for lead times extending to 3–4 years.

Disruptions to regular QBO cycling

The characteristic QBO descending eastward and westward wind pattern disintegrated in 2019/20 with unexpected westward winds appearing near 40 hPa along with an atypical ascending layer of eastward winds (Fig. 1a). The small vertical scale of the ascending eastward layer is unique in the QBO record. A decomposition of the QBO winds

into EOFs (Methods) quantifies this unusual vertical structure (Fig. 1b). The first two EOFs (encompassing the largest scale downward propagating structure of the QBO) typically explain over 90% of the vertical structure variance but their values drop drastically to ∼20% by May 2020 as the higher order, smaller scale, EOFs 3 and 4 grow in amplitude. This extreme 2019/20 decrease in the variance explained by EOFs 1 and 2 greatly exceeds the decrease to 60% associated with the 2015/16 disruption.

The overall rate of phase change of the QBO had been remarkably stable before the 2015/16 disruption (Fig. 1c). Constant QBO phase progression represented by the upper red line in Fig. 1c provides a reasonably accurate representation of the true phase from 1976 until the 2015/16 disruption with a standard deviation of the phase until then of ∼45°. The 2015/16 disruption resulted in a retrogressed phase shift of ∼135°, well outside this standard deviation. The lower red line denotes the post-disruption constant phase progression prediction, but this again failed in early 2020 when the QBO phase rapidly increased by ∼135°, returning close to the original phase that would be expected based on the historical phase progression (upper red line). Since there are only a few months where the phase has returned near the original prediction line, it remains to be seen exactly where the QBO phase will settle after this most recent disruption.

Canonical model vs. meridional wave fluxes

For both disruptions, strong wave-forcing by meridional momentum transport (meridional EP-flux; Methods) instigated an eastward-to-westward transition of the zonal-mean zonal winds in the lower stratosphere, around 40 hPa (Fig. 2). The canonical model of the QBO explains the oscillation as resulting from a feedback between the zonal-mean zonal wind and vertical momentum transport[21,22]. Momentum deposition by upward-propagating waves causes wind vertical shear zones to descend even as the Brewer-Dobson circulation moves the entire tropical stratosphere upward[13]. Beginning in June and lasting until September 2019, westward forcing by meridional momentum transport at 50 hPa was large compared to the net forcing from the canonical QBO model (Fig. 2a). In the context of the 1979–2020 ERA5 record this forcing was extremely large over all QBO altitudes below the descending westward shear zone (i.e. between 70 and 20 hPa; cf., red line and grey shading in Fig. 2c). In the canonical QBO model, waves deposit momentum in the zonal-mean flow over narrow altitude ranges, where they encounter strong vertical shears. However during July–September 2019 strong deposition occurred over

all altitudes of the QBO eastward phase, including those well below the descending westward shear zone (Fig. 2c).

Similar features are evident for the 2015/16 disruption (Fig. 2b,d), but with different timing. Strong forcing by meridional momentum transport at 50 hPa began in November 2015 and persisted through early February 2016 when westward winds emerged near 40 hPa (Fig. 2b). Again this forcing was extremely large in the context of the 1979–2020 record and it occurred within a deep eastward QBO phase (Fig. 2d). A shallow layer of westward wind shear centered at 50 hPa, that appeared in November 2015 and strengthened over the next 3 months, is clearly visible in the December–February average vertical profile (Fig. 2d, black line). In contrast, in July-September 2019 the beginning of a shear anomaly is only just discernible as an inflection point in the wind profile near 50 hPa (Fig. 2c, black line). The westward shear anomaly then gradually strengthened from September onward (Fig. S2a), until westward winds emerged near 40 hPa in late December 2019.

The 2019/20 QBO disruption thus resembles the 2015/16 event in that meridional momentum fluxes, neglected in the canonical QBO model, became anomalously strong and weakened the QBO eastward phase in the lowermost stratosphere, leading approximately three months later to the emergence of a shallow westward layer near 40 hPa. In both events this forcing occurred near the bottom of the eastward QBO phase, well below the descending westward phase above. The peak wind speed reached in the shallow westward layer was similar in both cases, being -21 m s^{-1} in 2019/20 and -19 m s^{-1} in 2015/16 (Fig. 2a,b). The two events differed in the timing of the strongest forcing by meridionally propagating waves: during Southern Hemisphere (SH) winter for the 2019/20 disruption, and during NH winter for the 2015/16 disruption. Forcing strengths also differed: peak forcing was stronger in 2015/16 (Fig. 2a and 2b, red lines) but concentrated over a shorter period from when the QBO eastward phase began its decay to when the 40 hPa westward layer emerged. At 50 hPa the time-integrated forcing from June to December 2019 was roughly 30% larger than that from October 2015 to February 2016 (-17 m s^{-1} and -13 m s^{-1}, respectively) though was spread over a longer period (Fig. S3). As with the EOF analysis, this suggests that the more recent disruption was the stronger of the two.

Role of Southern Hemisphere in 2019/20 disruption

Rossby waves propagate upward and equatorward from their extratropical source regions, but the tropical stratosphere is usually shielded from their incursions by a region of westward or weak eastward zonal wind in the subtropical stratosphere. This was the case near 20 hPa in July–September 2019 when the wind near 20° S was very strongly westward compared to the other years between 1979–2020 (Fig. 3a). In contrast, near 70 hPa the SH subtropical winds were very strongly eastward compared to other years (Fig. 3b). Consequently, this allowed for an exceptionally large northward wave-momentum flux (meridional EP-flux) from 20° S to the equator at 50 hPa (Fig. 3c). Since Rossby waves cannot propagate into the westward summer hemisphere winds, this caused large westward momentum flux convergence at the equator and corresponding westward tendency (Fig. 2a,c).

Similarly during the previous disruption equatorward wave propagation was inhibited during December-February 2015/16 by a westward NH subtropical barrier at higher altitudes (Fig. 3d) but favoured by NH subtropical winds at lower altitudes that were very strongly eastward compared to other years (Fig. 3e), allowing an anomalously large equatorward wave-momentum flux at 50 hPa (Fig. 3f). In contrast the equatorward flux from the NH in December–February 2019/20 was unremarkable, close to the median value for 1979–2020 (Fig. 3f), thereby confirming the importance of SH forcing for the 2019/20 event. Both disruptions occurred when subtropical winds favoured equatorward Rossby wave propagation at the lowermost altitudes of the QBO but not at higher altitudes. This explains why meridional momentum flux convergence did not occur at higher altitudes in the shear zones and accelerate their downward progression.

The SH winter of 2019 was unusual in that a rare minor sudden stratospheric warming (SSW) occurred, beginning in late August[7,8]. The timing of the warming roughly coincided with the peak westward forcing by meridional EP-flux in August and September (Fig. 2a). Concurrently, a large increase in tropical upwelling occurred, most likely due to the anomalous meridional overturning circulation associated with the SSW[23], leading to increased vertical advection at the equator near 40 hPa in September 2019 that contributed to the deceleration of the eastward QBO phase at that level (Fig. S2c). The displacement of the SH polar vortex during the minor warming may also have contributed to a subtropical corridor of eastward winds at 40–50 hPa over South America enabling

synoptic-scale wave propagation toward the equator in late August / early September, in a manner similar to that documented for the 2015/16 disruption[24]. However, further investigation will be required to determine whether or not the occurrence of the minor warming was essential to the 2019/20 QBO disruption. Nonetheless the common feature of both disruptions was the large equatorward meridional momentum fluxes, whatever their proximate causes.

Climate change

While the 2015/16 disruption could reasonably be judged as a "once in 50-year event" a second disruption suggests possible climate-change connections. In a warming climate the quasi-regular QBO cycling breaks down in some model projections but, in general, uncertainties in the representation of small scale gravity waves in models leads to a wide spread in QBO projections[25] and hence any projected changes in occurrences of disruptions are unreliable. On the other hand, in all multi-model QBO projections, there is an overall weakening of the oscillation in the lower stratosphere[25–27], attributed[26] to the well established speeding-up of the Brewer-Dobson circulation (tropical upwelling) in models in response to climate change[14]. A weaker QBO with eastward phase persisting longer in the lower stratosphere due to a faster Brewer-Dobson circulation is more likely to be vulnerable to the effects of extra-tropical wave fluxes penetrating the equatorial latitudes. In the climate model projections used for the latest IPCC assessment[28] this flux increases in winter and spring between the historical period 1961–2000 and 2061–2100 under Shared Socioeconomic Pathways[29] (SSP) 5-8.5 and 3-7.0 scenarios (Fig. 4). Interannual variability (standard deviation) of the monthly mean fluxes also increased, on average, and combined with the increase in the mean this implies a greater proportion of winters are likely to have sufficiently anomalous fluxes to disrupt the QBO. Robustness of the response for the mean is confirmed by remarkably similar results (not shown) obtained from idealised double and quadruple CO_2 simulations preformed for the SPARC (Stratospheric-Tropospheric Processes and their Role in Climate) QBO-initiative[30,31]. Using this novel approach of examining the more reliable response to climate change of the wave fluxes rather than the simulated QBOs per se, plus the already established speeding up of the Brewer-Dobson circulation[14] and weakening of QBO amplitudes[25–27], enables us to infer with some confidence that QBO disruptions are likely to become more common due a changing climate.

Discussion and Outlook

The quasi-biennial oscillation has been disrupted again for only the second time since its discovery. Both disruptions occurred near 40 hPa and were initiated by historically large forcing from extratropical waves. The 2019/20 event differs in that the dominant wave disturbances originated from the SH rather than the NH, no strong El Niño event was present, and an eastward jet subsequently emerged above the shallow westward layer.

The high predictability of the QBO on 3–4 year timescales can provide a source of long-term (seasonal to interanuual) predictive skill due to QBO teleconnections[1,11,12,32–35]. When this predictability disintegrates, as occurred in the 2015/16 and 2019/20 disruptions, the accuracy – and hence value to society – of such forecasts may be reduced. Following both disruptions the normal QBO cycling resumed, manifesting in 2020 as an eastward jet emerging above the shallow westward layer, consistent with the standard QBO paradigm (see Fig. S4) and auguring a return to the high predictability of the QBO until meteorological conditions once again favour disruption. As of September 2020 the QBO has returned to a typical eastward pattern.

Whether disruptions themselves can be predicted more than ~ 1 month in advance remains an open question[20]. The 2015/16 disruption was not predicted by operational seasonal forecasting systems[5] and early indications are that the same is true of the 2019/20 disruption, although models may perform better at predicting the evolution of the disruption once it has begun[20]. Predicting the full "life cycle" of QBO disruptions could provide a stringent test of models. Such work will be aided by the availability of new Aeolus satellite wind observations that will monitor the evolution of the QBO over the whole tropical belt[36]. Inherently shorter predictability of disruptions (as contrasted with the usual QBO) is consistent with their extratropical origins, since the extratropics are less predictable than the tropics.

Under climate change, Rossby wave propagation into the low-latitude stratosphere is expected to increase[37] and we have shown this occurs in model climate projections supporting the latest Intergovernmental Panel on Climate Change (IPCC) assessment. Under increasing influence from the extratropics, tropical stratospheric winds will likely become less predictable, leading to less skilful seasonal forecasts. Combined with an increas-

ing Brewer-Dobson circulation[14] and weakening QBO amplitudes[25–27], the prospect of QBO disruptions is likely to increase in a changed climate.

Methods

Our characterization of the QBO disruption is based on a tropical rawinsonde station (Singapore, 1°N, 104°E) and global gridded analysis fields (ERA5 reanalysis[38]).

Daily and monthly averages of the zonal wind component were constructed from the twice daily meteorological Singapore soundings[39]. The vertical structure (100–10 hPa) of the QBO was decomposed into a set of Empirical Orthogonal Functions (EOFs[16,17]) based on the monthly averages from Jan 1976–Dec 2014. The monthly winds from Jan 2013–Sep 2020 were then projected onto the first four leading EOFs as the Principal Components (PCs) and the relative variance explained by each of the PCs calculated for each month.

The ERA5 reanalysis combines a global atmospheric model with surface, aircraft, and satellite observations from 1979-present, resulting in an ongoing global, gridded, data set of winds and temperature that captures tropospheric weather systems, stratospheric waves and circulations, and the QBO[38]. These gridded meteorological fields (6-hourly in time, 2° horizontal and ∼0.5 km vertical) are used to calculate contributions to the zonal-mean zonal momentum budget due to wave forcing, quantified by the Eliassen-Palm (EP) flux, and advection[40]. Note that for these calculations the high vertical resolution model levels are used as reanalysis output on the standard available pressure levels have insufficient vertical resolution for accurate calculation of vertical wind shear and other vertical gradients involved in the momentum budget calculations.

Acknowledgments

ERA5 data were obtained from the Copernicus Data Store. The European Centre for Medium-Range Weather Forecasts (ECMWF) Operational Analysis data were obtained via the online portal (www.ecmwf.int/en/forecasts). The Singapore soundings were obtained from the NOAA IGRA2 data center. The climate model data used was obtained from the CMIP6 international archive:
https://esgf-index1.ceda.ac.uk/projects/cmip6-ceda/. NB was supported by the Met Office Hadley Centre Programme funded by BEIS and Defra and the UK-China Research

& Innovation Partnership Fund through the Met Office Climate Science for Service Partnership (CSSP) China as part of the Newton Fund. LC was supported by the NASA Modeling and Analysis Program. PN was supported by the NASA Atmospheric Composition Modeling and Analysis Program. SO was supported by the National Centre for Atmospheric Science and UK NERC (NE/P006779/1, NE/N018001/1). CW was funded by the Royal Society, University Research Fellowship (UF160545). TB was funded by an EPSRC Doctoral Training Account. We thank Adam Scaife for updating us on the UK Met Office Seasonal Forecasts for the 2019/2020 winter.

Author Contributions

JA, NB, LC, PN and SO designed the study, performed the analysis and drafted the paper. TB and CW provided input on wind observations and their interpretation.

References

1. Baldwin, M. P. *et al.* The quasi-biennial oscillation. *Rev. Geophys.* **39,** 179–229 (2001).
2. Ebdon, R. & Veryard, R. Fluctuations in equatorial stratospheric winds. *Nature* **189,** 791–793 (1961).
3. Reed, R. J., Campbell, W. J., Rasmussen, L. A. & Rogers, D. G. Evidence of a downward-propagating, annual wind reversal in the equatorial stratosphere. *Journal of Geophysical Research* **66,** 813–818 (1961).
4. Newman, P. A., Coy, L., Pawson, S. & Lait, L. R. The anomalous change in the QBO in 2015–2016. *Geophysical Research Letters* **43,** 8791–8797 (2016).
5. Osprey, S. M. *et al.* An unexpected disruption of the atmospheric quasi-biennial oscillation. *Science* **353,** 1424–1427 (2016).
6. Coy, L., Newman, P. A., Pawson, S. & Lait, L. R. Dynamics of the Disrupted 2015/16 Quasi-Biennial Oscillation. *Journal of Climate* **30,** 5661–5674 (2017).
7. Rao, J., Garfinkel, C. I., White, I. P. & Schwartz, C. The Southern Hemisphere Minor Sudden Stratospheric Warming in September 2019 and its Predictions in S2S Models. *Journal of Geophysical Research: Atmospheres* **125.** e2020JD032723 2020JD032723, e2020JD032723. eprint: `https://agupubs.onlinelibrary.wiley.com/doi/pdf/10.1029/2020JD032723`. `https://agupubs.onlinelibrary.wiley.com/doi/abs/10.1029/2020JD032723` (2020).

8. Shen, X., Wang, L. & Osprey, S. The Southern Hemisphere sudden stratospheric warming of September 2019. *Science Bulletin* (June 2020).
9. Tegtmeier, S. *et al.* Temperature and tropopause characteristics from reanalyses data in the tropical tropopause layer. *Atmospheric Chemistry and Physics* **20,** 753–770 (2020).
10. Bushell, A. C. *et al.* Evaluation of the Quasi-Biennial Oscillation in global climate models for the SPARC QBO-initiative. *Quart. J. Roy. Meteor. Soc.* **Accepted** (2020).
11. Anstey, J. A. & Shepherd, T. G. High-latitude influence of the quasi-biennial oscillation. *Quarterly Journal of the Royal Meteorological Society* **140,** 1–21 (2014).
12. Scaife, A. A. *et al.* Predictability of the quasi-biennial oscillation and its northern winter teleconnection on seasonal to decadal timescales. *Geophysical Research Letters* **41,** 1752–1758 (2014).
13. Dunkerton, T. J. The role of gravity waves in the quasi-biennial oscillation. *Journal of Geophysical Research: Atmospheres* **102,** 26053–26076 (1997).
14. Butchart, N. The Brewer-Dobson circulation. *Reviews of Geophysics* **52,** 157–184 (2014).
15. O'Sullivan, D. Interaction of extratropical Rossby waves with westerly quasi-biennial oscillation winds. *Journal of Geophysical Research: Atmospheres* **102,** 19461–19469 (1997).
16. Wallace, J. M., Panetta, R. L. & Estberg, J. Representation of the equatorial stratospheric quasi-biennial oscillation in EOF phase space. *J. Atmos. Sci.* **50,** 1751–1762 (1993).
17. Dunkerton, T. J. The quasi-biennial oscillation of 2015–2016: Hiccup or death spiral? *Geophysical Research Letters* **43,** 10, 547–10, 552 (2016).
18. Barton, C. A. & McCormack, J. P. Origin of the 2016 QBO Disruption and Its Relationship to Extreme El Niño Events. *Geophysical Research Letters* **44,** 11, 150–11, 157 (2017).
19. Hitchcock, P., Haynes, P. H., Randel, W. J. & Birner, T. The emergence of shallow easterly jets within QBO westerlies. *Journal of the Atmospheric Sciences* **75,** 21–40 (2018).

20. Watanabe, S., Hamilton, K., Osprey, S., Kawatani, Y. & Nishimoto, E. First Successful Hindcasts of the 2016 Disruption of the Stratospheric Quasi-biennial Oscillation. *Geophysical Research Letters* **45,** 1602–1610 (2018).

21. Lindzen, R. & Holton, J. R. A theory of the quasi-biennial oscillation. *J. Atmos. Sci.* **25,** 1095–1107 (1968).

22. Holton, J. R. & Lindzen, R. S. An updated theory for the quasi-biennial cycle of the tropical stratosphere. *J. Atmos. Sci.* **29,** 1076–1080 (1972).

23. Baldwin, M. P. *et al.* Sudden Stratospheric Warmings. *Earth and Space Science Open Archive,* 49 (2020).

24. Lin, P., Held, I. & Ming, Y. The Early Development of the 2015/16 Quasi-Biennial Oscillation Disruption. *Journal of the Atmospheric Sciences* **76,** 821–836 (2019).

25. Richter, J. H. *et al.* Response of the Quasi-Biennial Oscillation to a warming climate in global climate models. *Quarterly Journal of the Royal Meteorological Society* **n/a** (2020).

26. Kawatani, Y. & Hamilton, K. Weakened stratospheric quasibiennial oscillation driven by increased tropical mean upwelling. *Nature* **497,** 478 (May 2013).

27. Butchart, N. *et al.* QBO Changes in CMIP6 Climate Projections. *Geophysical Research Letters* **47,** e2019GL086903 (2020).

28. Eyring, V. *et al.* Overview of the Coupled Model Intercomparison Project Phase 6 (CMIP6) experimental design and organization. *Geoscientific Model Development* **9,** 1937–1958. `https://gmd.copernicus.org/articles/9/1937/2016/` (2016).

29. Gidden, M. J. *et al.* Global emissions pathways under different socioeconomic scenarios for use in CMIP6: a dataset of harmonized emissions trajectories through the end of the century. *Geoscientific Model Development* **12,** 1443–1475. `https://gmd.copernicus.org/articles/12/1443/2019/` (2019).

30. Butchart, N. *et al.* Overview of experiment design and comparison of models participating in phase 1 of the SPARC Quasi-Biennial Oscillation initiative (QBOi). *Geoscientific Model Development* **11,** 1009–1032. `https://www.geosci-model-dev.net/11/1009/2018/` (2018).

31. Anstey, J. A., Butchart, N., Hamilton, K. & Osprey, S. M. The SPARC Quasi-Biennial Oscillation initiative. *Quarterly Journal of the Royal Meteorological Society* **n/a.** eprint: `https://rmets.onlinelibrary.wiley.com/doi/pdf/10`

.1002/qj.3820. https://rmets.onlinelibrary.wiley.com/doi/abs/10.1002/qj.3820.

32. Scaife, A. A. *et al.* Skillful long-range prediction of European and North American winters. *Geophysical Research Letters* **41,** 2514–2519. eprint: https://agupubs.onlinelibrary.wiley.com/doi/pdf/10.1002/2014GL059637. https://agupubs.onlinelibrary.wiley.com/doi/abs/10.1002/2014GL059637 (2014).

33. Son, S.-W., Lim, Y., Yoo, C., Hendon, H. H. & Kim, J. Stratospheric Control of the Madden–Julian Oscillation. *Journal of Climate* **30,** 1909–1922. eprint: https://doi.org/10.1175/JCLI-D-16-0620.1. https://doi.org/10.1175/JCLI-D-16-0620.1 (2017).

34. Gray, L. J. *et al.* Surface impacts of the Quasi Biennial Oscillation. *Atmospheric Chemistry and Physics* **18,** 8227–8247. https://www.atmos-chem-phys.net/18/8227/2018/ (2018).

35. Mundhenk, B. D., Barnes, E. A., Maloney, E. D. & Baggett, C. F. Skillful empirical subseasonal prediction of landfalling atmospheric river activity using the Madden–Julian oscillation and quasi-biennial oscillation. *npj Climate and Atmospheric Science* **1,** 2397–3722. https://doi.org/10.1038/s41612-017-0008-2 (2018).

36. Witschas, B. *et al.* First validation of Aeolus wind observations by airborne Doppler Wind Lidar measurements. *Atmospheric Measurement Techniques Discussions,* 1–23 (2020).

37. Shepherd, T. G. & McLandress, C. A Robust Mechanism for Strengthening of the Brewer–Dobson Circulation in Response to Climate Change: Critical-Layer Control of Subtropical Wave Breaking. *Journal of the Atmospheric Sciences* **68,** 784–797 (2011).

38. Hersbach, H. *et al.* The ERA5 global reanalysis. *Quarterly Journal of the Royal Meteorological Society* (2020).

39. Durre, I., Xungang, Y., Vose, R. S., Applequist, S. & Arnfield, J. Integrated Global Radiosonde Archive (IGRA), Version 2. *NOAA National Centers for Environmental Information.* Accessed May 2020 (2016).

40. Andrews, D. G., Holton, J. R. & Leovy, C. B. *Middle Atmosphere Dynamics* (Academic, San Diego, Calif., 1987).

41. Dee, D. P. *et al.* The ERA-Interim reanalysis: Configuration and performance of the data assimilation system. *Quarterly Journal of the royal meteorological society* **137,** 553–597 (2011).

42. NCAS British Atmospheric Data Centre. *European Centre for Medium-Range Weather Forecasts: ECMWF operational analysis: Assimilated Data* 2006. `http://catalogue.ceda.ac.uk/uuid/c46248046f6ce34fc7660a36d9b10a71` (2020).

43. Hendon, H. H. & Wheeler, M. C. Some space–time spectral analyses of tropical convection and planetary-scale waves. *Journal of the atmospheric sciences* **65,** 2936–2948 (2008).

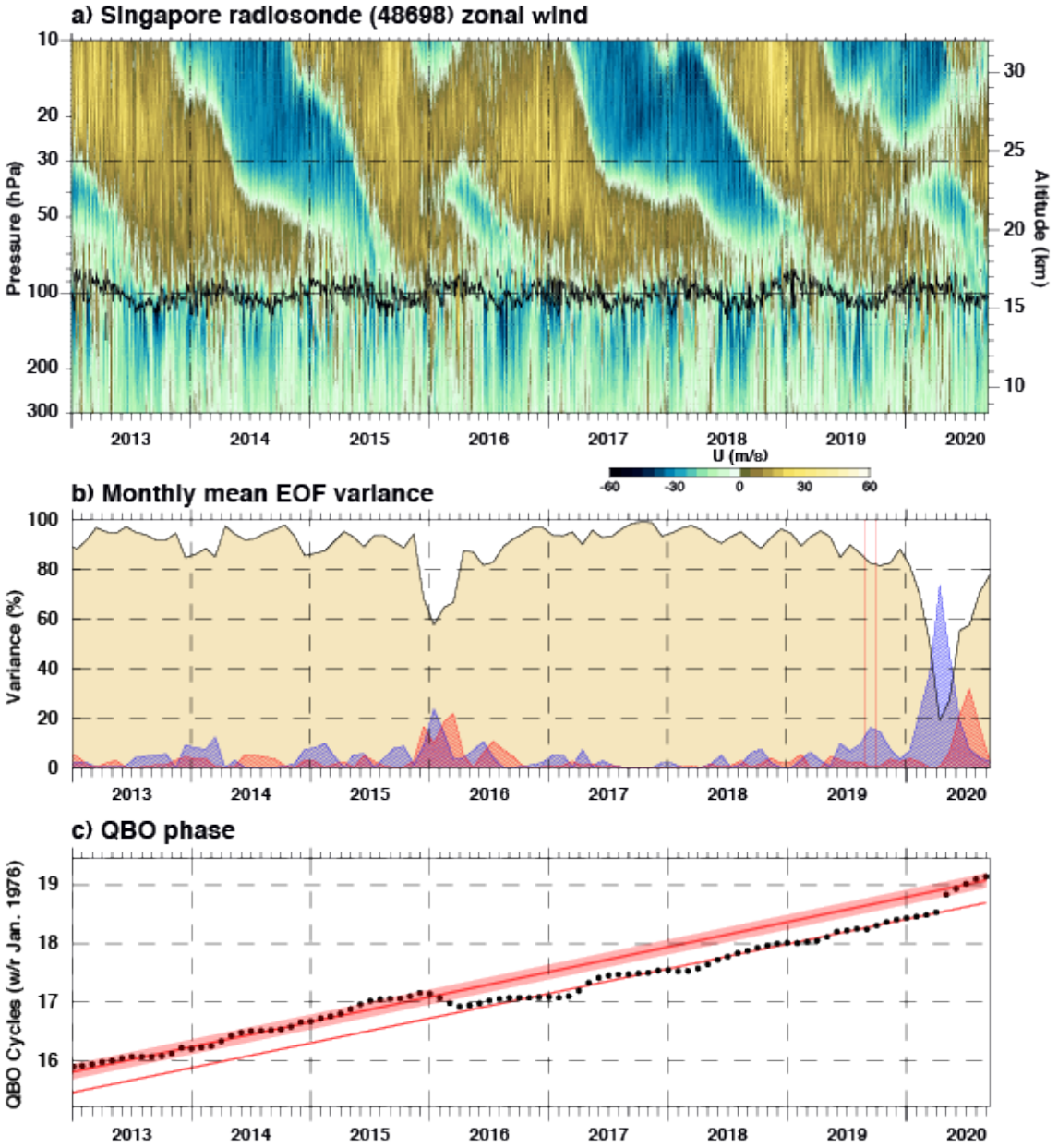

Figure 1. (a) Twice daily radiosonde zonal wind observed at Singapore (1.4° N, 104° E, station id 48698). Lapse-rate tropopause determined from the radiosonde temperatures is shown as a black line. Missing radiosonde data are filled in with MERRA-2 interpolated to the location of Singapore. (b) The percent variance explained by principal components (PCs) 1 and 2 combined (black curve) and PCs 3 (red curve) and 4 (blue curve) as a function of time based on the monthly averaged Singapore zonal wind profiles (1976–2020) from 100–10 hPa. The EOF calculation was based on monthly averaged winds limited to 1976–2014 to avoid the two disruptions. The red vertical lines bracket September 2019. (c) Singapore QBO phase as a function of time in units scaled so that each 2π is one QBO cycle. The upper red line is fitted to the the phase from January 1976 through December 2014. The lower red line is fitted from August 2016 through December 2019. The shading about the upper red line denotes plus or minus one standard deviation. (For the complete time series going back to January 1976, see Fig. S1.)

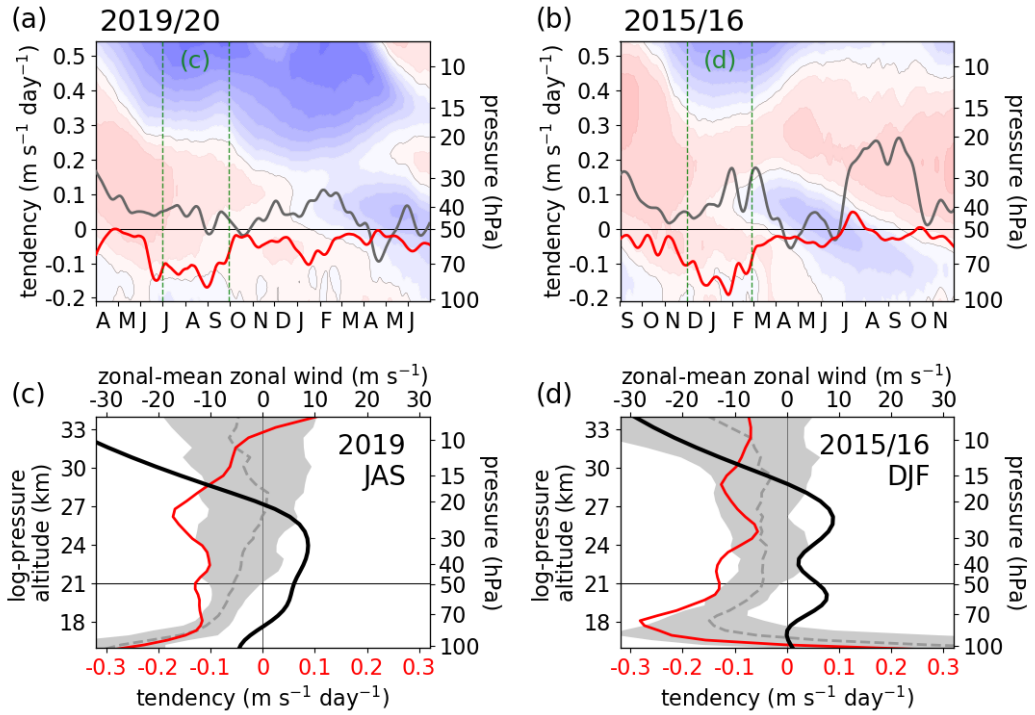

Figure 2. (a,b) Time series of ERA5 equatorial forcing tendencies due to meridional EP-flux convergence (red) and the sum of vertical EP-flux convergence and vertical advection (grey) superimposed on the altitude vs. time progression of zonal-mean zonal wind (5 m s^{-1} contours, eastward red, westward blue) for (a) the 2019/20 disruption and (b) the 2015/16 disruption. (c,d) Vertical profiles of meridional EP-flux convergence (red) and zonal-mean zonal wind (black) averaged over (c) July 2019 to September 2019 and (d) December 2015 to February 2016; the averaging periods are bracketed by vertical dashed green lines in (a,b). Grey shading shows the 5%–95% range (median dashed) of meridional EP-flux convergence over the 1979–2020 period for (c) July–September (JAS) and (d) December–February (DJF). All panels use ERA5 daily data, 4° S–4° N average, smoothed in (a,b) with a 5-day (31-day) running mean for wind (tendencies). (For the the full momentum budget, see Fig. S2.)

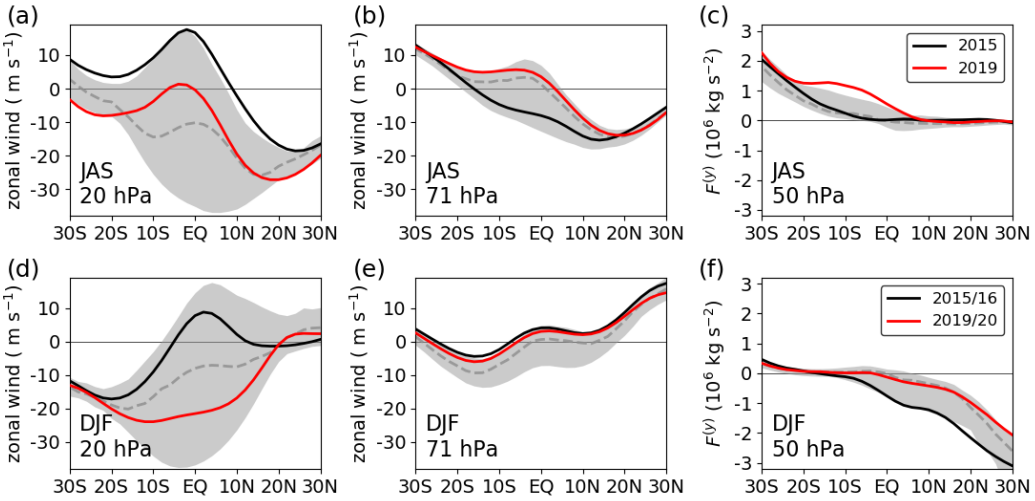

Figure 3. Meridional profiles of ERA5 (a,b) zonal-mean zonal wind and (c) meridional EP-flux, averaged over July–September (JJA) at the indicated pressure levels. (d,e,f) As (a,b,c) but averaged over December–February (DJF). The most recent (red) and previous (black) disruption years are highlighted in each panel. Grey shading shows the 5%–95% range (median dashed) over the 1979–2020 period for each variable at the indicated level and months.

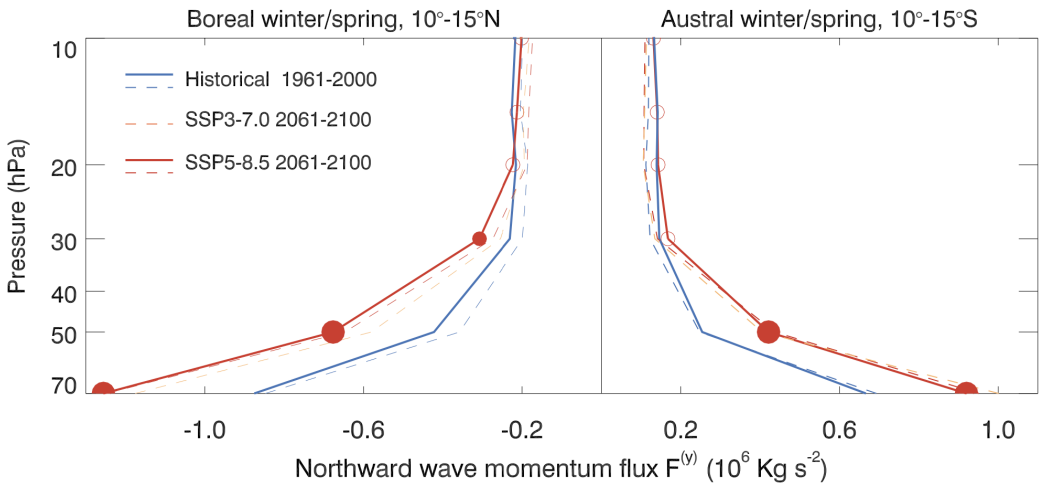

Figure 4. Solid lines: Multi-model mean vertical profiles of northward wave momentum flux averaged over 10–15° N for NH winter and spring (December-May, left side) and 10–15° S for SH winter and spring (June-November, right side) for ten models that provided wave flux diagnostics for the historical and SSP5-8.5 scenario simulations for phase six of the Coupled Model Intercomparison Project[28]. Dashed lines: Multi-model means for the subset of six models that also provided data for the SSP3-7.0 scenario. Only one realization was used per model. Circles indicate data levels and are filled when the difference between the historical and SSP5-8.5 model ensembles are significant at 95% (large circles) and 90% (small circles), based on a Students t-test. Models that provided data were: **CanESM5**, **CESM2**, **CESM2-WACCM**, GFDL-CM4, GFDL-ESM4, HadGEM3-GC31-LL, **INM-CM4-8**, MIROC6, **MRI-ESM2-0**, **UKESM1-0-LL**, with names in bold indicating the model provided data for both scenarios.

Supplemental

Fig. S1 shows the full 1976–2020 progression of QBO phase using Singapore radiosonde winds, of which a subset is shown in Fig. 1c. The linear slope over most of the record indicates the usual high predictability of QBO phase. The 2015/16 and 2019/20 disruptions appear as abrupt deviations from the usual phase progression.

Fig. S2 compares the evolution of ERA5 zonal-mean zonal wind and its vertical shear in the 2015/16 and 2019/20 disruption events (Fig. S2a,b) and details of the zonal-mean zonal momentum budget at 41 hPa and 50 hPa (Fig. S2c–f). More precisely the pressure levels shown are 40.53 and 49.60 hPa, the closest ERA5 levels to 40 and 50 hPa. The resolved forcing terms are the meridional EP-flux component, vertical EP-flux component, meridional advection, and vertical advection. Forcings are smoothed with a 31-day running mean as in Fig. 2a,b. The canonical model forcing shown in Fig. 2a,b (grey line) is the sum of the vertical EP-flux and vertical advection at 50 hPa as shown in Fig. S2e,f. The time axis in Fig. S2 places the "central date" of each disruption at the same relative position on the axis for both disruptions. This is the time at which ERA5 zonal-mean zonal winds turned westward at 40 hPa, determined as 21 December 2019 and 1 February 2016 for the two events. For the 2019/20 disruption, ERA5 data are extended slightly in time using ECMWF operational analysis[41,42].

Fig. S3 shows the time integral of forcing tendency due to meridional EP-flux for the two disruptions. The total forcing by horizontal wave-momentum flux provides an alternate metric for the "strength" of the disruption, complementary to the EOF-based metric shown in Fig. 1b.

Fig. S4 illustrates the resumption of the standard QBO mechanism following the 2019/20 disruption. Strong meridional momentum fluxes induce a departure from typical QBO behaviour, but in their absence the canonical QBO model is robust. Following the emergence of shallow 40 hPa westward winds in the two disruption events, forcing by meridional EP-flux drops (Fig. 2a and Fig. 2b, red line), as expected since these winds present a barrier to Rossby waves. They also are a barrier to upward-propagating tropical waves that would otherwise force the descent of the overlying westward QBO phase, which then stalls and is carried upward by the Brewer-Dobson circulation (Fig. 2a,b). The lower-level westward winds then descend in the characteristic QBO manner. When

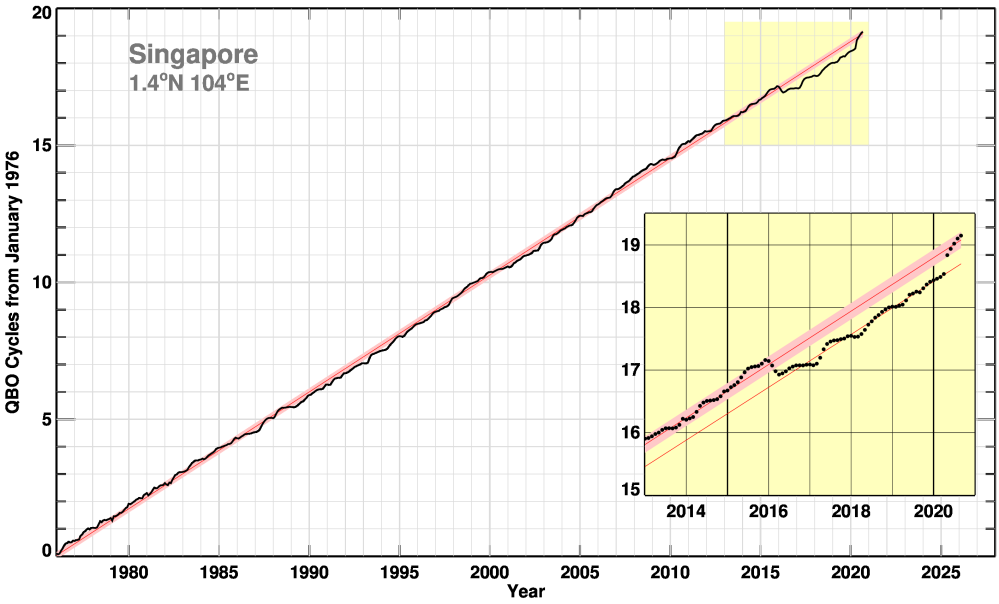

Figure S1. Singapore QBO phase as in Fig. 1c, but showing the full record since January 1976.

they reach ∼ 70 hPa, any barrier to upward-propagating waves with eastward phase speeds is removed, and eastward wave forcing becomes available aloft. Following 2015/16 disruption this led to the resumption of eastward phase descent in April 2016, forced by the canonical QBO model forcing terms (Fig. 2b). The aftermath of the 2019/20 disruption unfolded similarly, but with a distinct twist: an eastward jet emerged in May 2020 from the remnants of the stalled westward phase near 25 hPa. This was forced by the vertical EP-flux component (Fig. S4), of which ∼50% is due to large-scale waves ($k = 1$–10; not shown), consistent with radiative damping of Kelvin waves as they encounter eastward wind shear. The rapid (sub-monthly) variations seen in Singapore observations in this region (Fig. 1a) are also consistent with Kelvin wave activity[43].

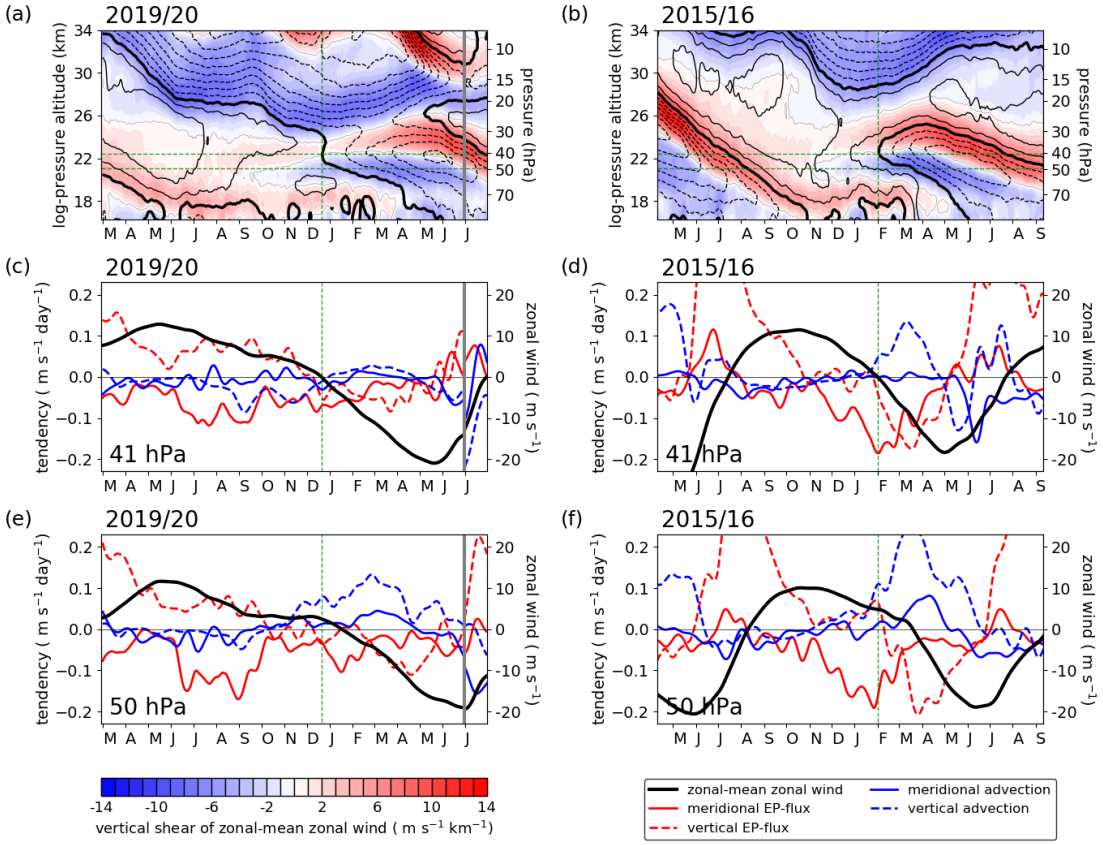

Figure S2. QBO disruptions as seen in the ERA5 reanalysis during (a,c,e) 2019/20 and (b,d,f) 2015/16. (a,b) Zonal-mean zonal wind (black contours; zero thick, westward dashed, 5 m s^{-1} spacing) and its vertical shear (filled contours). (c,d) Zonal-mean zonal wind tendency due to eddy momentum transports and advection, and zonal-mean zonal wind (thick black line) at 41 hPa. (e,f) As (c,d), but at 50 hPa. Vertical green dashed lines marks the time when westward winds first emerge near 40 hPa for each disruption. Horizontal green dashed lines in (a,b) indicate 41 and 50 hPa, the altitudes shown in (c–f). All panels use daily ERA5 daily, 4° S–4° N average, smoothed with (a,b) 5-day running mean, (c–f) 31-day running mean. ERA5 data are extended in time using ECMWF operational analysis (transition marked by grey vertical line in panels a,c,e).

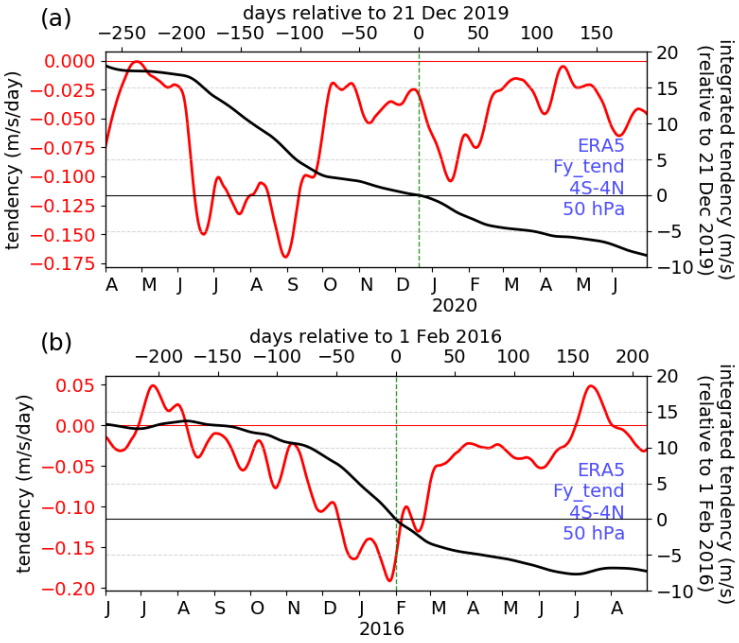

Figure S3. (a) Time-integrated zonal-mean zonal wind tendency (black) due to forcing by meridional EP-flux (red) for the 2019/20 disruption. Red curve is the same as in Fig. 2a (50 hPa, 4° S–4° N, daily ERA5 data smoothed with 31-day running mean). The black curve is the time integral of the red curve. (b) As (a) but for the 2015/16 disruption. Red curve is the same as in Fig. 2b.

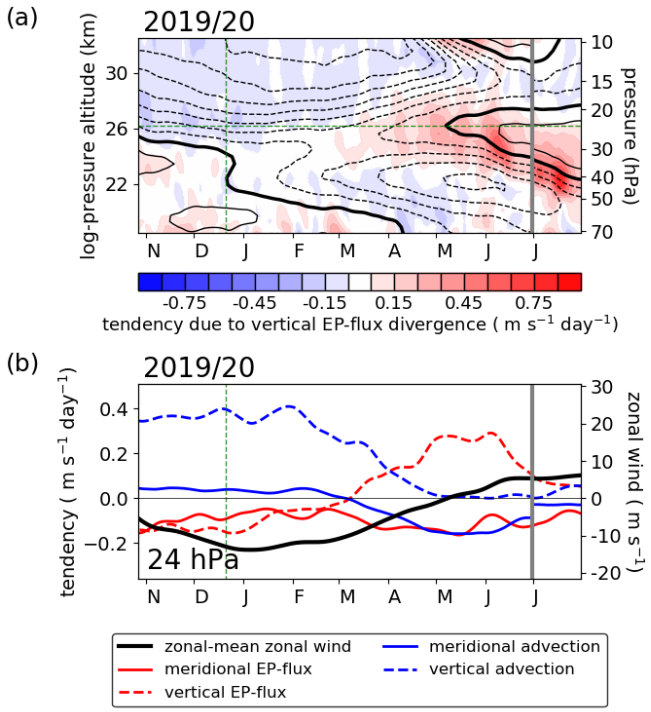

Figure S4. (a) Zonal-mean zonal wind (black contours; zero thick, westward dashed, 5 m s^{-1} spacing) and wind tendency due to vertical EP-flux component (filled contours). (b) Zonal-mean zonal wind tendency due to eddy momentum transports and advection, and zonal-mean zonal wind (thick black line), at the altitude of emerging eastward winds. Vertical green dashed line marks the time when westward winds first emerge near 40 hPa. Horizontal green dashed line in (a) indicates the altitude shown in (b). All panels use daily ERA5 daily, 4° S–4° N average, smoothed with (a) 11-day running mean, (b) 31-day running mean. ERA5 data are extended in time using ECMWF operational analysis (transition marked by grey vertical line in panels a, b).